ELSEVIER

Journal of Alloys and Compounds 330–336 (2002) 590–596

Journal of ALLOYS AND COMPOUNDS

www.elsevier.com/locate/jallcom

Hydrogen absorption and electrochemical properties of $Mg_{2-x}Ni$ ($x=0$–0.5) alloys prepared by bulk mechanical alloying

Toshiro Kuji[a,*], Hiroaki Nakano[b], Tatsuhiko Aizawa[c]

[a]*Corporate R&D Center, Mitsui Mining and Smelting Co. Ltd., 1333-2 Haraichi, Ageo, Saitama 362-0021, Japan*
[b]*School of High-Technology for Human Welfare, Tokai University, 317 Nishino, Numazu, Shizuoka 410-0395, Japan*
[c]*Research Center for Advanced Science and Technology, The University of Tokyo, 4-6-1 Komaba, Meguro-ku, Tokyo 153-8904, Japan*

Abstract

Thermodynamic properties of hydrides of $Mg_{2-x}Ni$ alloys produced by bulk mechanical alloying were determined from the pressure–composition isotherms for absorption over the temperatures from 623 to 423 K. The van't Hoff plots for the plateau pressures of the isotherms clearly indicated the existence of high- and low-temperature hydrides with different entropy and enthalpy for hydride formation. The phase transition temperature was 525 K for $Mg_{2.0}Ni$ and decreased with increasing value of x. Chemical and electrochemical behaviors of $Mg_{2-x}Ni$ alloys in an alkaline solution were precisely determined. It was found that hydrogen absorption in $Mg_{2-x}Ni$ alloys takes place by only immersing the alloys in 6 M KOH solution. On the other hand, during electrical charging hydrogen content increased with the quantity of charged electricity and reached the maximum value. However, the hydrogen content decreased afterwards because the corrosion of the alloys in the alkaline solution is significant.

Keywords: Mg–Ni alloy; Bulk mechanical alloying; Hydrogen solubility; Allotropic transformation

1. Introduction

Mg–Ni alloys have attracted growing interest as one of the most important hydrogen storage alloys forming Mg_2NiH_4 hydride corresponding to a hydrogen content higher than 3 wt.%. Recently a mechanical alloying technique has been utilized due to the importance of nano-structural control for improving the hydrogen absorbing properties of Mg–Ni alloys [1–4]. In previous studies, we demonstrated synthesis of nano-structural $Mg_{2-x}Ni$ alloys by the bulk mechanical alloying (BMA) technique based on the repeated forging processes within one-fiftieth of the process time reported in conventional ball milling type mechanical alloying [4].

Recent crystallographic studies revealed that there are two allotropic ternary hydrides represented in Mg_2NiH_4, suggesting that this allotropic phase transition is due to a hydrogen order/disorder phenomena [5]. However, the thermodynamic properties of the hydrides have not well been determined, especially reports on the thermodynamic behavior corresponding to the allotropic phase change of the hydrides have not been found in the literature.

In this paper, the difference in the thermodynamic properties between the high and low temperature hydrides will be discussed in relation to the hydrogen order/disorder phenomena presumed by studies on the structure of $Mg_{2.0}Ni$ hydrides.

Moreover, in the second part of this paper, the chemical and electrochemical properties of $Mg_{2-x}Ni$ alloys will be discussed. It is very much important to understand the behavior of Mg–Ni alloys in an alkaline solution when clarifying the potentiality of the Mg–Ni alloys in Ni–MH batteries. In this study, the anomalous behavior, which has not been observed for AB_5 and AB_2 [6,7] types of alloys will be discussed with regard to the reaction of Mg with water.

2. Experimental

Elemental magnesium flakes (99.9%, <1 mm) and nickel powders (99.9%, <200 μm) were pre-mixed and poured into a die cavity. The amount of alloy to be prepared was 25 g. The mixture of powders were repeatedly extruded and compressed by a maximum applied load of 500 kN in the die cavity placed on a high-speed forging machine [4]. In this study, the mixture of Mg and Ni

*Corresponding author.
E-mail address: t_kuji@mitsui-kinzoku.co.jp (T. Kuji).

0925-8388/02/$ – see front matter
PII: S0925-8388(01)01594-8

powders was processed for 1500–2000 extrusion–compression cycles. During the repeated cycles, the relative density of consolidated compact was kept constant at approximately 80% of the ingot value. Lubricants were not used for BMA for the $Mg_{2-x}Ni$ alloys. The forging facilities and cyclic schedule have been described in detail elsewhere [4,8].

The phase and microstructure of the synthesized $Mg_{2-x}Ni$ alloys were characterized by X-ray diffraction (XRD) and transmission electron microscopy (TEM). The pressure–composition (P–C) isotherms for absorption were determined using a Sievert's apparatus at 423 to 623 K.

In this study, the chemical behavior of $Mg_{2-x}Ni$ alloys with KOH and water were examined. The alloys of 1 g were immersed in 200 ml of 6 M KOH or distilled water for a prescribed time. After drying, the alloys were heated up to 873 K in a Horiba hydrogen analyzer (EMGA-621) to determine the amount of hydrogen uptake during the immersion.

Alloy electrodes were prepared from a mixture of alloy powders (<300 mesh), Ni powders and PTFE (polytetrafluoroethylene) in a ratio of 15.4:80.9:4.0. The mixture was processed to a sheet form and then the sheet was crushed to powder. For using the powders as a alloy electrode, the powders were then packed into a small pocket, 15×15 mm, made of nickel net. Electrical charging and discharging characteristics of $Mg_{2-x}Ni$ alloy electrodes were determined with a constant current density of 17 mA/g in a electrolyte cell. The cell consisted of two vessels with a gas burette so that the hydrogen gas generated during charging could be collected in the gas burette. The real amount of electrochemically absorbed hydrogen [7,9] then can be calculated by subtraction of the amount of charged electricity required for hydrogen gas generation from the integrated current over the electrochemical process.

3. Results and discussion

3.1. Structure of synthesized $Mg_{2-x}Ni$ alloys

Fig. 1 shows the powder XRD patterns of synthesized $Mg_{2-x}Ni$ alloys after 2000 forging and compression cycles. Diffraction peaks from $Mg_{2.0}Ni$ dominate the XRD patterns over the diffraction scan, suggesting that the elemental powders were well mechanically alloyed, although some very small Ni diffraction peaks still remained. The lattice parameters of the hexagonal Mg_2Ni compound were calculated from the XRD pattern of $Mg_{2.0}Ni$ alloy, i.e. $a=0.5243$ nm and $c=1.334$ nm. These are in good agreement with values previously reported [10]. The diffraction peaks from $Mg_{1.75}Ni$ and $Mg_{1.5}Ni$ alloys are somewhat broadened, implying the existence of an amorphous phase in these alloys. According to the

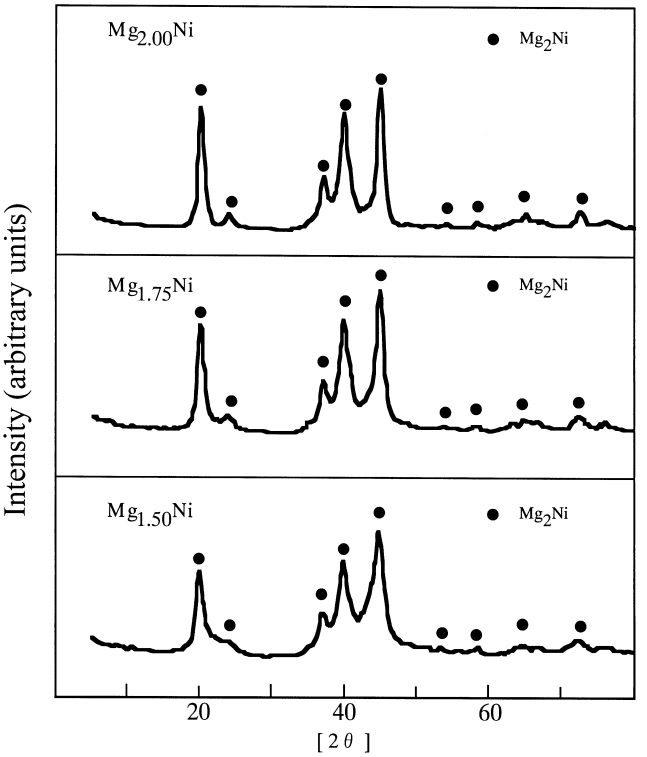

Fig. 1. X-Ray diffraction patterns of $Mg_{2-x}Ni$ alloys.

Mg–Ni equilibrium phase diagram, a corresponding amount of $MgNi_2$ Laves phase should be detected in $Mg_{1.75}Ni$ and $Mg_{1.5}Ni$ alloys. However, as mentioned above, the XRD patterns for both alloys were dominated by the peaks from Mg_2Ni compound, suggesting that excess amount of Ni could dissolve in Mg_2Ni phase without losing Mg_2Ni lattice symmetry. It should be mentioned that 2000 BMA cycles correspond to 4.4 h of processing time, which is much shorter than that for the conventional ball milling type MA, i.e. more or less 200 h for synthesizing Mg_2Ni alloy. This could be a great advantage of BMA for industrial applications.

Fig. 2 shows TEM images and diffraction patterns of synthesized Mg_2Ni and $Mg_{1.5}Ni$ alloys. From the lattice image, the grain size of Mg_2Ni phase could be estimated at more or less 10 nm, which is in good agreement with the value calculated from the XRD peak width using Scherrer's equation. The lattice image of $Mg_{1.5}Ni$ alloy implies that the alloy could be partially amorphized as expected from XRD results.

3.2. Thermodynamic properties of the hydrides

In order to obtain the hydrogen absorption behavior of nano-structured $Mg_{2-x}Ni$ alloys, P–C isotherms were determined at 423–623 K, as shown in Fig. 3. Plateaux corresponding to the hydride formation clearly appeared on each isotherm. The maximum hydrogen concentration decreases with increasing value of x. In the plateau region

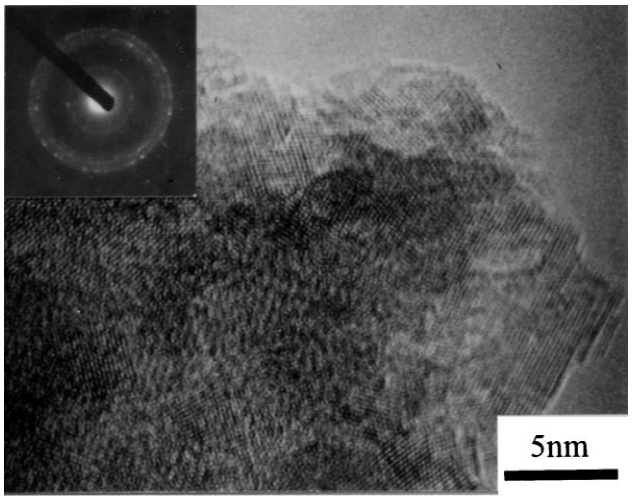

$Mg_{2.0}Ni$

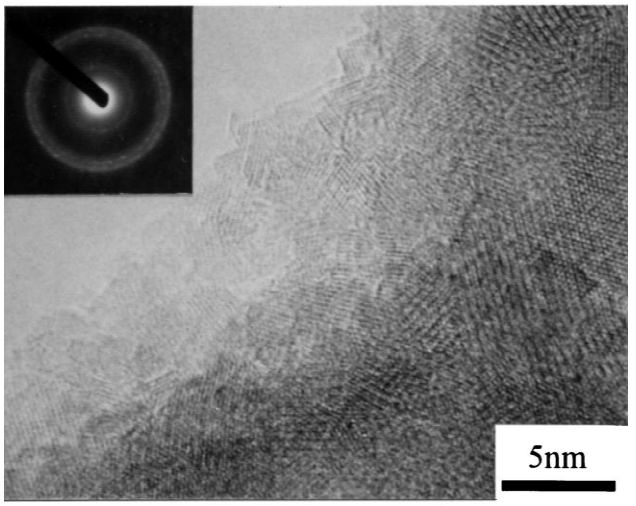

$Mg_{1.5}Ni$

Fig. 2. Transmission electron micrographs of $Mg_{2.0}Ni$ and $Mg_{1.5}Ni$ alloys prepared by BMA.

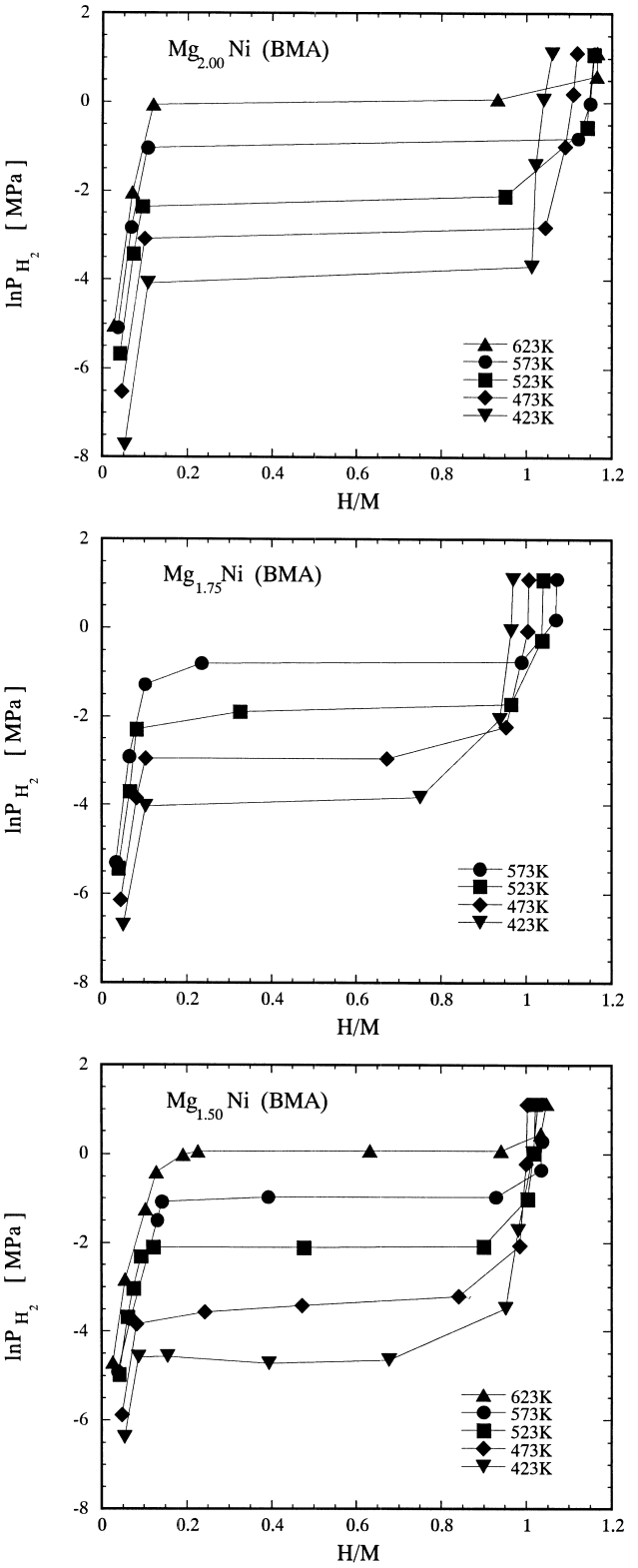

Fig. 3. P–C isotherms for $Mg_{2-x}Ni$ alloys.

hydride coexists with $Mg_{2.0}NiH_{\alpha}$ solid solution. It seems that the hydrogen concentration corresponding to the phase boundary on the hydride side decreases with decreasing temperature so that plateau is wider at higher temperatures. This is obvious for the alloys with lower Mg content at lower temperatures. In most case for alloy–hydrogen systems, i.e. AB_5 and AB_2 types of alloys, the width of the plateau becomes narrower with increasing temperature. This opposite is true for the Mg_2Ni hydride formation because it is accompanied by a structure change and the allotropic phase transition exists in the Mg_2Ni hydride. On the other hand, the phase boundary on Mg_2NiH_{α} side is relatively insensitive to temperature, implying no structure change in solid solution region. In fact, the logarithmic plot of equilibrium pressures versus the reciprocal temperature at $H/Mg_2Ni=0.05$ yields a good straight line over the experimental temperatures, see Fig. 4.

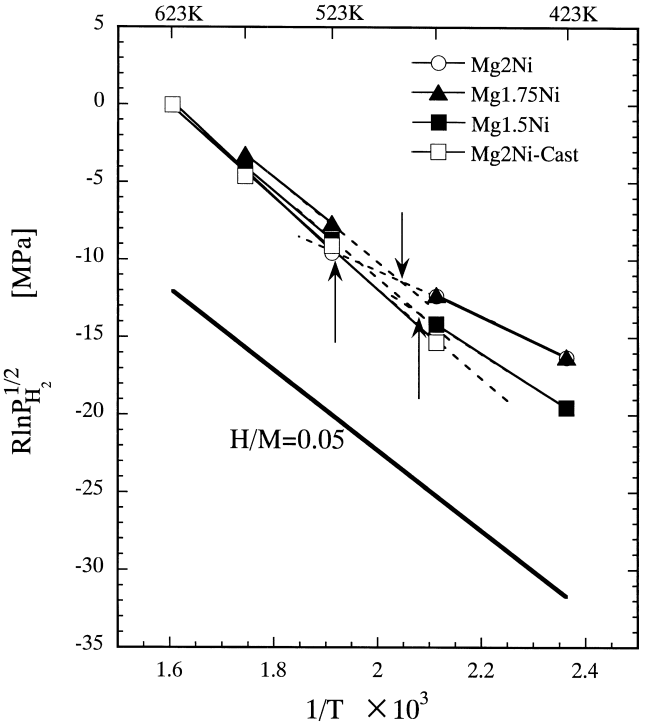

Fig. 4. van't Hoff plot for $Mg_{2-x}Ni$ alloys.

The thermodynamic behaviors for the hydride formation were determined by plotting logarithmic plateau pressures against the reciprocal temperature (van't Hoff plot), as shown in Fig. 4. It can be clearly seen that the linearity changes between low and high temperature regions, implying that a phase transition occurs in the hydride, and the transition temperature decreases with decreasing Mg content in the alloys. The entropy and enthalpy values for hydride formation calculated from the linearity of the van't Hoff plots are tabulated in Table 1. The values for HT are found to be in relatively good agreement with those of the previous work [11]. In any alloy composition, both entropy and enthalpy for the high-temperature hydride (HT) are more negative than those for the low-temperature hydride (LT).

In order to understand the above phenomena, the hypothetical transition from HT to LT was considered. At first, the plateau pressure for the high-temperature hydride was extrapolated to a temperature below the transition temperature, T_f. Then this hypothetical hydride transforms to the low-temperature hydride. This transformation is accompanied with a increase in plateau pressure and decrease in hydrogen concentration at the phase boundary on the hydride side of plateau. In the present study, a schematic illustration of the change in chemical potential for the transition from high temperature to low temperature hydrides were proposed in Fig. 5 which satisfies the experimental results without any inconsistency.

Furthermore, the transition from HT to LT is due to the ordering of hydrogen atoms on four of six available sites in the high temperature hydride [5] so that it should occur with an increase in the partial molar entropy of hydrogen in the LT Mg_2NiH_4 hydride. This could be a dominant contributor to the difference in plateau pressure between high- and low-temperature hydrides. On the other hand, at this moment it is almost impossible to estimate the quantitative change in partial molar enthalpy of hydrogen with hydrogen ordering because the structure of the LT hydride phase has not been well determined. The phase equilibria of hydrogen in the Mg_2Ni alloy are summarized in the phase diagram as shown in Fig. 6. It should be noted again that the $\alpha/\alpha+\beta$ region becomes narrower and the transition temperature from HT to LT hydrides decreases with decreasing Mg content in the alloys.

It is of interest that van't Hoff plot for cast Mg_2Ni does not show any linearity change over the experimental temperatures (Fig. 4), giving similar thermodynamic values to those calculated from HT. Further investigations concerning the electronic structures of the LT and HT phases are planned [12].

Table 1
Enthalpy and entropy values for the hydride formation

	$-\Delta H_f$ (kJ/mol H)		$-\Delta S_f$ (kJ/mol H)		T_f (K)
	HT	LT	HT	LT	
$Mg_{2.00}Ni$	31.3	15.7	50.3	20.9	511
$Mg_{1.75}Ni$	26.6	15.9	43.1	21.4	480
$Mg_{1.50}Ni$	29.1	19.5	47.2	27.5	476
$Mg_{2.00}Ni$(cast)	29.7		47.5		

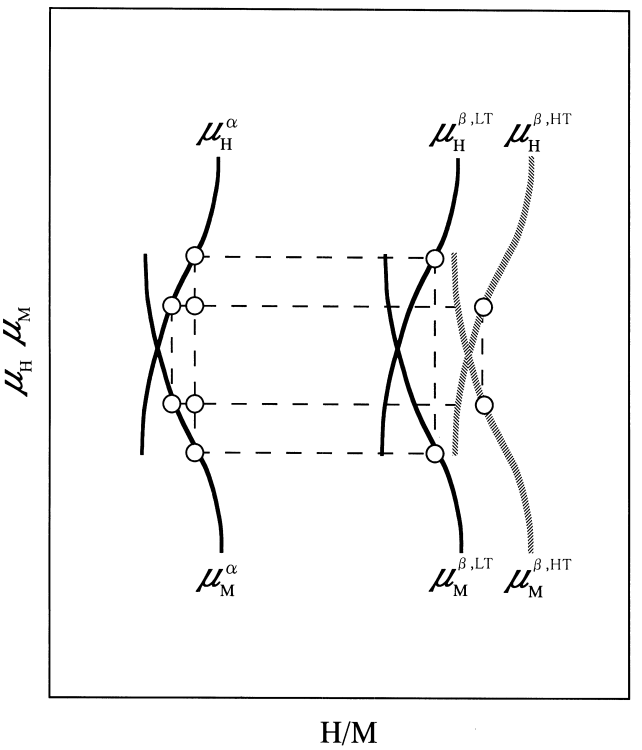

Fig. 5. Schematic illustration on the change in chemical potential for the transition from high temperature and low temperature hydrides. $\mu_H^{\beta,HT}$ and $\mu_M^{\beta,LT}$ are hypothetical chemical potentials of hydrogen and metal at $T<T_f$, respectively.

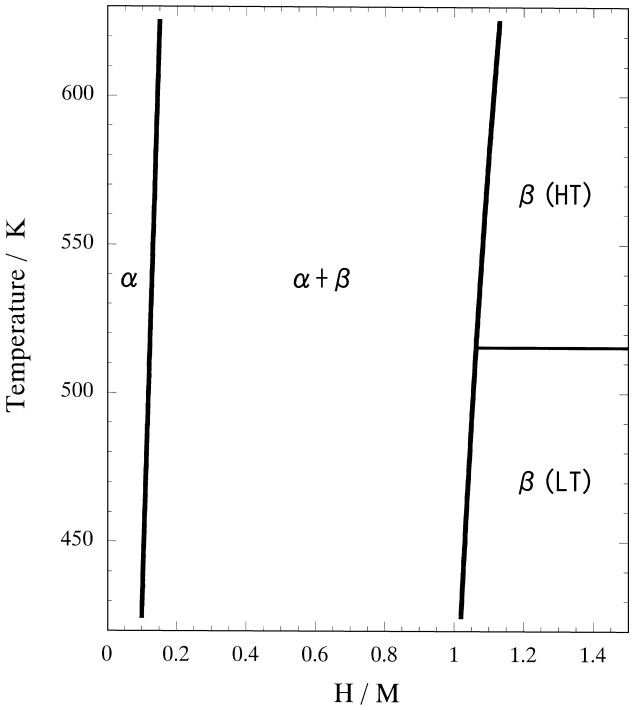

Fig. 6. Phase diagram for Mg_2Ni–H system.

3.3. Chemical and electrochemical properties of synthesized $Mg_{2-x}Ni$ alloys

In this study, it was found that synthesized $Mg_{2-x}Ni$ alloys were easily hydrogenated by simply immersing alloys in 6 M KOH solution, as shown in Fig. 7a. The absorbed hydrogen concentration (H/M) increased with immersing time and reached H/M=0.11, 0.23 and 0.26 for $Mg_{2.0}Ni$, $Mg_{1.75}Ni$ and $Mg_{1.5}Ni$, respectively, after 44 h of immersion. Almost the same amount of hydrogen was absorbed in cast Mg_2Ni. The immersion of the Mg_2Ni alloy in distilled water resulted in a higher hydrogen concentration, i.e. H/M=0.21 after 44 h of immersion (Fig. 7b). In this case, the pH value of water rose from 6.8 to 11.2 within several minutes after starting immersion and did not change much afterwards.

The above results lead to the mechanism on hydrogen absorption during immersing alloys in the alkaline solutions as follows. If Mg is immersed in an alkaline solution, hydrogen gas generation and $Mg(OH)_2$ formation take place [13], but these reactions terminate soon after immersion because the Mg surface is coated with $Mg(OH)_2$. The pH value of distilled water after immersing alloys was almost identical to that calculated from the solubility of $Mg(OH)_2$ [14] so that $Mg(OH)_2$ could also form on the $Mg_{2-x}Ni$ alloy surfaces (Eq. (1)):

$$Mg_{2-x}Ni + 2(2-x)OH^- = (2-x)Mg(OH)_2 + Ni + 2(2-x)e^- \quad (1)$$

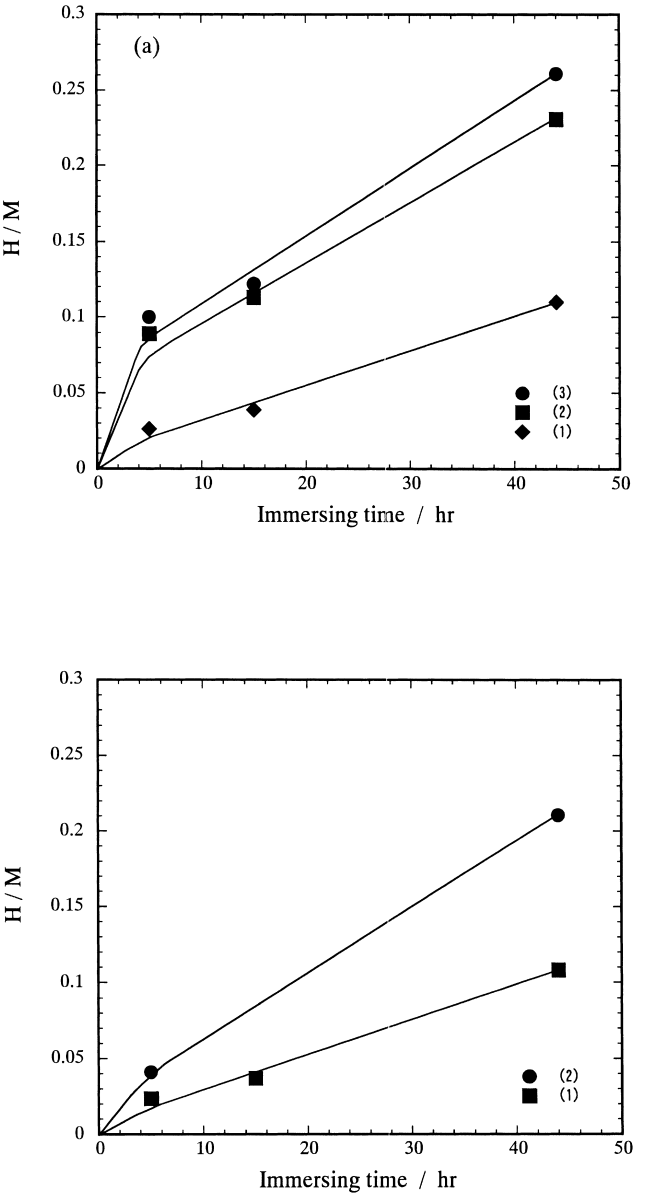

Fig. 7. Change in hydrogen content in the alloy powders with immersing time. (a) In 6 M KOH; 20°C; alloy powder 1.0 g; KOH 200 ml; (1) $Mg_{2.00}Ni$; (2) $Mg_{1.75}Ni$; (3) $Mg_{1.5}Ni$. (b) Comparison between 6 M KOH and distilled water for cast Mg_2Ni alloy powder; 20°C; alloy powder 1.0 g, KOH or water 200 ml; (1) in 6 M KOH; (2) in water.

The electrons produced by $Mg(OH)_2$ formation are supplied to water on Ni surface which could act as a catalyst for the hydrogen absorption [15] and hydrogen is formed as follows by Eq. (2):

$$\begin{array}{l}(2-x)H_2\\ \uparrow\\ 2(2-x)H_2O + 2(2-x)e^- = 2(2-x)H + 2(2-x)OH\\ \downarrow\\ 2(2-x)H_{abs}\end{array} \quad (2)$$

This hydrogen (H) is absorbed in $Mg_{2-x}Ni$ alloys.

However, when the alloys are saturated by hydrogen, hydrogen gas (H_2) is subsequently generated. The OH^- ion concentration in water is lower than in KOH so that the equilibrium described in Eq. (2) is liable to proceed in the right direction. That could be the reason why the higher hydrogen concentration is obtained by immersion in water than in KOH.

Fig. 8a shows the electrical charging characteristics of $Mg_{2-x}Ni$ alloy electrodes for the first charging cycle. The initial current efficiency was almost 100% for all electrodes, implying that 100% of the charged current is spent for the hydrogen absorption. However, after the hydrogen concentration reached the maximum, it decreased linearly with increasing charged quantity of electricity. The reduction in the hydrogen concentration became obvious with increasing Ni content of the alloys. This anomalistic behavior is not observed for AB_5, AB_2 [6,7] and AB types of alloy. The maximum hydrogen concentration increased with increase in x value, i.e. 243 mAh/g at $x=0$, 292 mAh/g at $x=0.25$ and 379 mAh/g at $x=0.5$. These values are much lower than the maximum hydrogen concentrations obtained from P–C isotherms, shown in Fig. 3. It should be mentioned that the maximum hydrogen concentration for the second charging cycle apparently decreased, i.e. 201 mAh/g for Mg_2Ni to 287 mAh/g for $Mg_{1.5}Ni$.

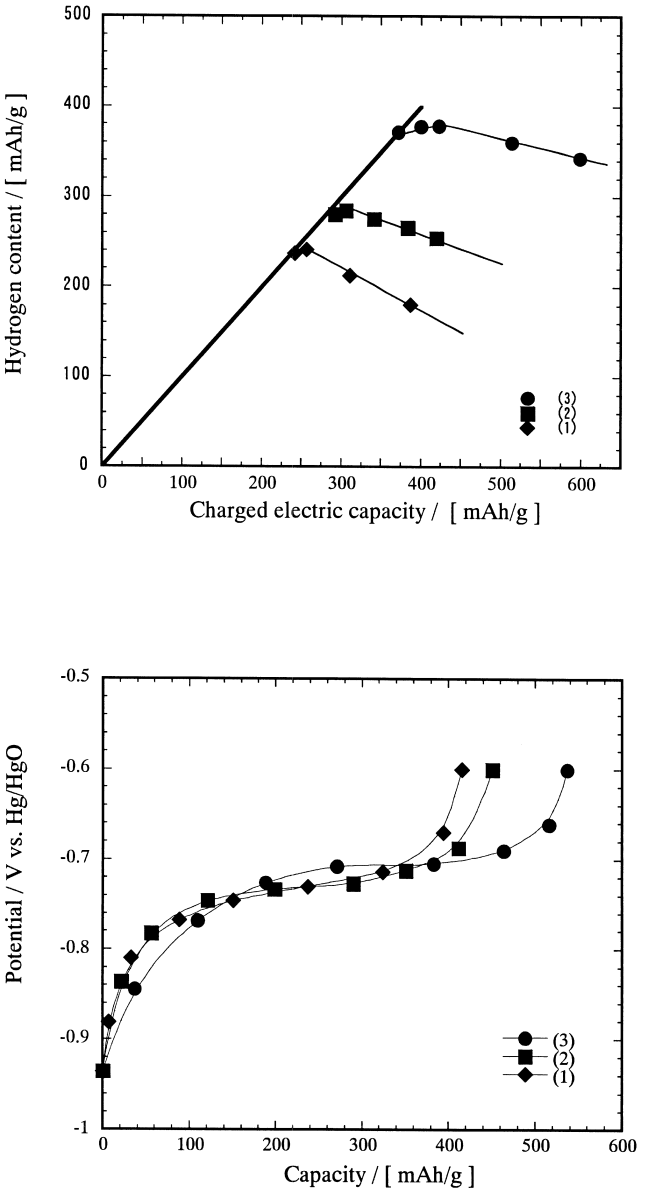

Fig. 8. Charge/discharge characteristics. (a) Charging process; (b) discharging process. Current density 17 mA/g; 25°C. (1) $Mg_{2.00}Ni$; (2) $Mg_{1.75}Ni$; (3) $Mg_{1.5}Ni$.

Fig. 8b shows the first discharging curves, obtained immediately after the first charging shown in Fig. 8a. The discharging capacities increased with increasing x value, i.e. 414 mAh/g at $x=0$ and 534 mAh/g at $x=0.5$. It should be noticed that these values are much larger than the maximum hydrogen concentrations obtained during the charging process. Moreover, only 200 mAh/g of the second discharging capacity was obtained for each alloy, which was substantially lower than the first discharging capacity. In the case of the first charging–discharging cycle, the discharging capacity was much higher than the hydrogen concentration obtained during the charging process.

The reduction in the hydrogen concentration with proceeding charging process could be due to the generation of hydrogen gas by Eq. (2). As mentioned previously, the hydrogen concentration in the alloys was calculated by subtraction of the quantity of charging electricity corresponding to the hydrogen gas generation from the integrated current. However, if the amount of hydrogen gas generated by the corrosion of the alloys (Eq. (2)) during the charging process becomes noticeably large, it becomes impossible to determine the hydrogen solubility obtained purely by the electrical charging. This suggests that this extra amount of hydrogen is possibly counted in a discharging capacity. This could be the reason why the first discharging capacity was significantly larger than maximum hydrogen concentration as shown in Fig. 8a and b. During the first charging–discharging cycle, the alloys were severely corroded. Especially, during the discharging process, the alloys are anodically polarized so that the corrosion would fatally proceed. Therefore, the maximum hydrogen concentration obtained by the second charging process is markedly reduced and as a result only a small discharge capacity was obtained. A surface modification to prevent Mg–Ni alloys from corrosion is essential for battery applications.

4. Conclusions

Nanocrystalline $Mg_{2-x}Ni$ alloys were prepared by the BMA technique based on repeated extrusion–compression cycles. The van't Hoff plot for plateau pressures from the

P–C isotherms clearly described the allotropic phase transition in Mg_2NiH_4 hydride. In this study, the thermodynamic properties of both high-temperature and low-temperature hydrides were determined, which have not previously been reported in the literature. The transition temperature decreased with increasing Ni content in the alloys. In the Mg_2Ni–H system, it seems that the plateaux are narrower at lower temperatures due to the existence of the low temperature hydride. In this study, a quantitative phase diagram for the $Mg_{2-x}Ni$–H system and the relation of the chemical potentials between the both phases were proposed.

From the chemical and electrochemical properties, it was found that the $Mg_{2-x}Ni$ alloys were easily hydrogenated by simply immersing alloys in 6 M KOH and even in distilled water. This could be caused by the severe corrosion of the alloys, which is accompanied with the $Mg(OH)_2$ formation on the alloy surfaces.

The electrical charging and discharging behavior of the alloys were determined. In the first charging process, the initial current efficiency was almost 100% but after reaching the maximum hydrogen concentration, it decreased with an increase in the charged quantity of electricity. Moreover, it was found that the first discharging capacity was significantly larger than the hydrogen concentration obtained by the first charging. This anomalous behavior could be interpreted by the fact that the amount of hydrogen generated by the corrosion of alloys is substantially large during the charging–discharging cycles.

Acknowledgements

The authors would like to thank Mr. Nakayama and Ms. Hanzawa, Corporate R&D Center, Mitsui Mining & Smelting Co. Ltd. for careful measurements of P–C isotherms and high-resolution TEM observations.

References

[1] S. Orimo, H. Fujii, J. Alloys Comp. 232 (1996) L16.
[2] Z. Dehouche, R. Djaozandry, J. Goyette, T.K. Bose, J. Alloys Comp. 288 (1999) 312.
[3] T. Spassov, U. Koster, J. Alloys Comp. 287 (1999) 243.
[4] T. Aizawa, T. Kuji, H. Nakano, J. Alloys Comp. 291 (1999) 248.
[5] J. Schefer, P. Fischer, W. Halg, F. Stucki, L. Schlapbach, J.J. Didisheim, K. Yvon, J. Less-Common Met. 74 (1980) 65.
[6] H. Nakano, I. Wada, S. Wakao, J. Adv. Sci. 4 (1992) 242, (Japanese).
[7] H. Nakano, S. Wakao, J. Alloys Comp. 231 (1995) 587.
[8] T. Aizawa, C. Zhou, Adv. Eng. Mater. 2 (2000) 29.
[9] H. Nakano, S. Wakao, T. Shimizu, J. Alloys Comp. 253–254 (1997) 609.
[10] K.H. Buschow, Solid State Commun. 17 (1975) 891.
[11] P. Selvam, B. Viswanathan, C.S. Swamy, V. Srinivasan, Int. J. Hydrogen Energy 13 (1988) 87.
[12] H. Blomqvist, E. Ronnebro, D. Noreus, T. Kuji, J. Alloys Comp., in press.
[13] M. Pourbaix, Atlas of Electrochemical Equilibria in Aqueous Solution, National Association of Corrosion Engineers, Houston, TX, USA, 1974, p. 139.
[14] Handbook of Chemistry, The Chemical Society of Japan, 1972, p. 649.
[15] F. Meli, L. Schlapbach, J. Less-Common Met. 172–174 (1991) 1252.